proceedings

MDPI

Proceedings

PsInSAR Processing for Volcanic Ground Deformation Monitoring Over Fogo Island

Arun Babu [1,*] and Shashi Kumar [1]

[1] Photogrammetry and Remote Sensing Department, Indian Institute of Remote Sensing, ISRO, Dehradun, India; arunlekshmi1994@gmail.com, shashi@iirs.gov.in

* Correspondence: arunlekshmi1994@gmail.com; Tel.: +91-807-546-6497

Published: 8 June 2019

Abstract: Persistent Scatterer SAR interferometry (PsInSAR) has been widely used in the precise measurement of ground deformation due to anthropogenic and natural disturbance of the earth's surface. The present study has utilized the spaceborne C-band Sentinel-1 data for PsInSAR processing to generate a displacement map due to the volcanic eruption of Pico do Fogo volcano of the Fogo Island. An eruption was recorded in the year 2014-15 and the Fogo volcano became active on November 23, 2014. It was observed that the intensity of volcanic eruption during 2014-15 had approached the intensity of the volcanic eruption of 1951 which was recorded as one of the strongest eruptions on the island. The volcanic eruption was continued for 77 days and it had stopped on February 8, 2015. To find the mean line of sight displacement from PsInSAR processing a total of 7 SLC products of Sentinel-1 data in the interferometric mode was used. The SLC product of the SAR data which was acquired before starting the volcanic eruption was chosen as the master image and all the remaining 6 slave images were precisely coregistered. Selection of persistent scatterers (PS) is the most important step in PsInSAR processing. The initial set of PS was identified by amplitude stability index and the phase analysis was performed to estimate the phase stability of each resolution cell. After PS identification, 3D phase unwrapping was performed. The unwrapping step had involved the low-pass filtering of the complex phase difference and time series in the frequency domain using a Gaussian window. The phase difference between each filtered data point is then calculated. The unwrapped phase of the interferogram was used to generate a displacement map for the volcanic field. The PsInSAR based line of sight displacement was measured in the range of -34 mm to +35 mm and the standard deviation of the displacement was ranging from +2 mm to +30 mm.

Keywords: PSInSAR, Interferometric Wide, Amplitude Dispersion Index, Deformation

1. Introduction

Persistent Scatterer Interferometry is an advanced SAR interferometric technique capable of estimating surface deformations with millimetre level accuracy [1]. Conventional InSAR has the potential to estimate surface deformations. However, the high temporal decorrelation in the interferograms caused by the vegetation limits the capability of InSAR for estimating deformation of natural terrains. The accuracy of the InSAR is also affected by the phase delay introduced by the atmospheric constituents which are difficult to remove from the interferograms [2]. PSInSAR technique utilizes a large number of interferometric pairs compared to InSAR to overcome these limitations. Persistent Scatterers are the ground targets which exhibits amplitude and phase stability in all the datasets. PSInSAR uses these stable scatterers to effectively estimate and remove the atmospheric and topographic artefacts from the interferograms. The resulting differential interferograms contain only the residual phase due to surface deformations [3]. The PSInSAR technique is proved for its potential for volcanic deformation estimation[4], [5].

Pico do Fogo, on Fogo Island (Figure. 1 published by [6]), is the most active volcano and the highest peak in the Cape Verde archipelago and in the Central Atlantic oceanic region. It is formed as the African Plate moved towards the east over the hotspot and is the youngest volcano in the Cape Verde Islands. There happened roughly 26 eruptions in the previous 500 years [7]. Fogo erupted on 23rd November 2014 breaking its 20 years of quiescence since 1995. The eruption lasted for 77 days till February 2015 causing massive destruction to the nearby areas. On 28th November 2014, the lava flow through a linear fissure completely destroyed the Portela and Bangaeria villages nearby the volcano [6].

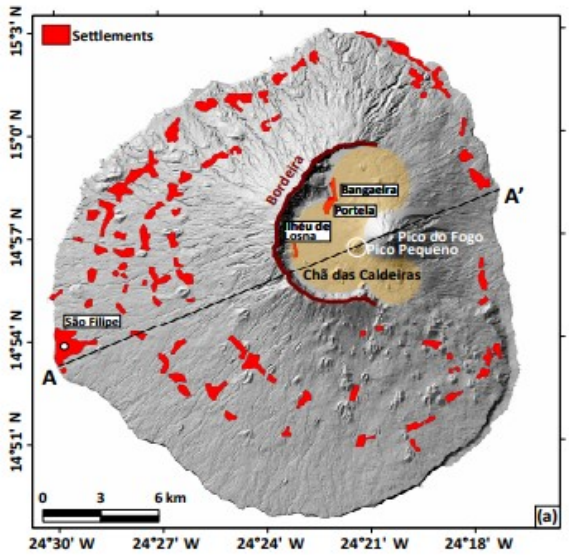

Figure. 1. Map of Fogo Island

The Sentinel-1A satellite is launched by the European Space Agency (ESA) on 3rd April 2014. It is having a C-band SAR antenna. Sentinel-1A is acquiring datasets with a new acquisition mode called as the Terrain Observation and Progressive Scan (TOPS) Mode which is a modified form of ScanSAR mode TOPS mode is very suitable for interferometric applications [8]. The Fogo volcano eruption episode is the first surface deformation activity acquired by the Sentinel-1A since its launch. The data sets acquired by Sentinel-1A in TOPS mode during the volcano episode period is used for PSInSAR processing [9].

2. 2. Dataset and Method

Seven scenes of Sentinel-1A acquired in Interferometric Wide (IW) TOPS mode VV polarization acquired in ascending pass from 3rd November 2014 to 15th March 2015 is used for this study. TOPS Mode acquires data in three sub-swaths covering a total swath of 250 km with a ground range cell size of 5 x 20 m. TOPS mode achieves uniform Distributed Target Ambiguity Ratio and Signal to Noise Ratio by steering the radar beam from backwards to forward electronically in azimuth direction in addition to the steering of the beam in range direction as in normal ScanSAR mode. Each sub-swath is a collection of bursts where each burst is an independent SLC image. In each sub-swath, these bursts are arranged in the order in an azimuth-time domain with black line separation in between the bursts. Before using the datasets for PSInSAR study data preprocessing has to be done which includes two steps. The first step is to extract the sub-swath covering the study area using the split operation and the second step is the removal of black strips in between the bursts by running a moving window averaging filter

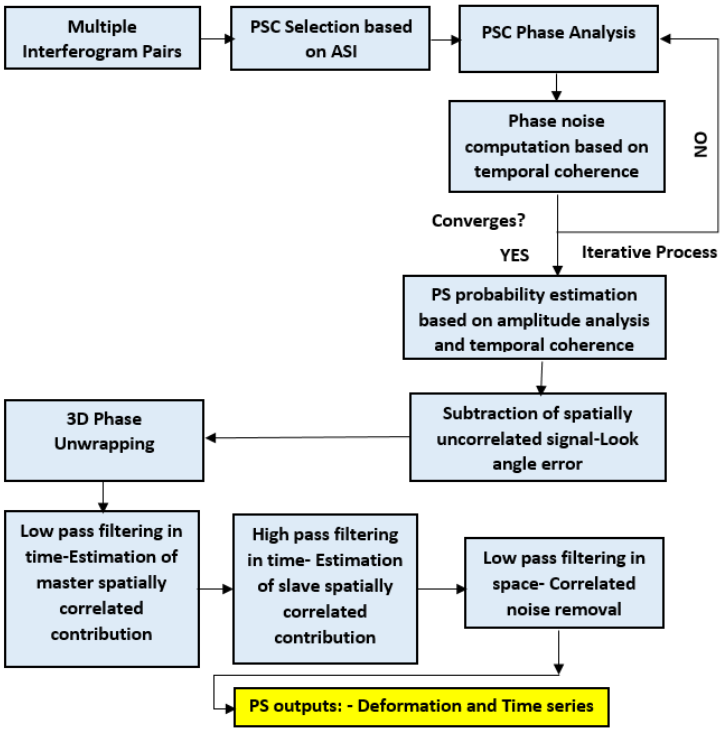

Figure. 2. Process Flow Chart

through all the bursts called as the deburst operation [8]. The dataset of 3rd November 2014 is set as the master image and the remaining images are set as the slave images. The maximum spatial and temporal baselines to the master image are 92 meters and 132 days respectively.

The process starts by selecting the image of 3rd November as the master image and all the remaining 6 slave images are coregistered with respect to the image taken as the master. Co-registration aligns the slave images with respect to the master image with sub-pixel level accuracy. It is done to provide backscatter information from the same ground target. After coregistration, the interferograms are formed taking the phase difference between each slave and the master image. 'N' interferograms can be formed with 'N+1' datasets. PSInSAR processing is done as per the flowchart is shown (Figure. 2).

The persistent Scatterers are the ground targets with high phase stability. The phase stability can be determined only after removing the undesired phase components namely APS, DEM- errors, terrain deformations and orbital ramps. Since targets with very less geometric and temporal decorrelation are required, pixels with stable amplitudes should be selected as Persistent Scatterer Candidates.

A subset of pixels from the PSC can be selected as the final persistent scatterers after estimating the phase stability of these pixels. Amplitude dispersion Index (D_A) is used to select the amplitude stable pixels [1], [4], [10].

$$D_A = \frac{\sigma_A}{\mu_A} \tag{1}$$

Equation 1 shows the formula for Amplitude Dispersion Index. σ_A is the temporal standard deviation of each pixels in all the datasets and μ_A is the temporal mean of each pixels in all the datasets. The amplitude dispersion and phase dispersion are in very good agreement for low values of Amplitude dispersion Index approximately up to 0.25 [1]. Amplitude dispersion index is used here to select the Persistent Scatterer Candidates for phase analysis, so a higher threshold of 0.4 is used here to select a large number of pixels.

Consider a PSC (x) in the ith interferogram which is corrected for topographic errors, the interferometric phase of this PSC can be written as [4], [11]:

$$\phi_{int,x,j} = W\{\phi_{def,x,i} + \phi_{a,x,i} + \phi_{orb,x,i} + \phi_{\varepsilon,x,i} + n_{x,i}\} \tag{2}$$

Where, $\phi_{def,x,i}$ is the surface deformation phase component, $\phi_{a,x,i}$ is the atmospheric phase delay component, $\phi_{orb,x,i}$ is phase component due to orbital errors, $\phi_{\varepsilon,x,i}$ is the look angle errors phase component and $n_{x,i}$ is the noise. W represents the wrapped operator. The phase contributions due to the surface deformation, atmosphere and orbit are spatially correlated so these three components are estimated using a filtering in spatial domain using a band pass filter. The look angle error is estimated by correlating it with the perpendicular component of baseline.

After correcting the spatially correlated phase components and the look angle error of all PSC the temporal coherence (γ) of all PSC is calculated to estimate the phase noise level [4], [11].

$$\gamma_x = \frac{1}{N}\left|\sum_{i=1}^{N} exp\{\phi_{int,x,i} - \bar{\phi}_{int,x,i} - \Delta\hat{\phi}_{\varepsilon,x,i}\}\right| \tag{3}$$

Equation (3) represents the temporal coherence of a PSC (x). Where N represents the number of interferograms, $\bar{\phi}_{int,x,i}$ is the estimated spatially correlated components and $\Delta\hat{\phi}_{\varepsilon,x,i}$ is the estimated look angle error. The PSC with high temporal coherence (γ_x) are selected as the new PSC and the remaining PSC are rejected. All the first four phase components in equation (2) is then re-estimated for this selected PSC and the process is repeated iteratively by dropping PSC based on the above criteria till the last noise term of equation (2) decreases and converges so that the temporal coherence of the PSC dominates the remaining small noise.

Amplitude dispersion index and temporal coherence are used together to select the final set of persistent scatterers (PS) from the PSC. For this requirement, Persistent Scatterer Probability is estimated for the PSC. At the last step, the PS points dominated by scatterers in neighbouring pixels

and PS points persistent only in certain interferograms are discarded. The remaining pixels are chosen as the final Persistent Scatterers for surface deformation estimation [11].

Due to the spatially uncorrelated component of look angle error, the interferometric phase difference between adjacent PS pixels may be greater than π. The slave and master contributions of look angle error estimated earlier are removed from the wrapped phase before phase unwrapping[11].

The wrapped phase is then unwrapped using 3D phase unwrapping technique. In the 3D phase unwrapping, two dimensions are in a spatial domain and one dimension is in the time domain. First phase differences of each PS pixels in time domain have to be estimated and later spatial phase unwrapping is performed for each time step of a particular PS pixel using an iterative algorithm. Once the phase of each PS pixels is unwrapped in all the interferograms it is then integrated in time. For accurate phase unwrapping the deformation between a PS pixel and one of its neighbouring PS pixels should be less than half of the antenna wavelength either in space or time[11].

The unwrapped phase contains phase components due to spatially correlated look angle error, atmosphere and orbital errors. These spatially correlated phase components have very low temporal coherence son they are estimated by using a high pass phase filtering in the temporal domain followed by low pass phase filtering in the spatial domain. The remaining interferometric phase contains the only phase due to surface deformation [11].

3. Results and Discussions

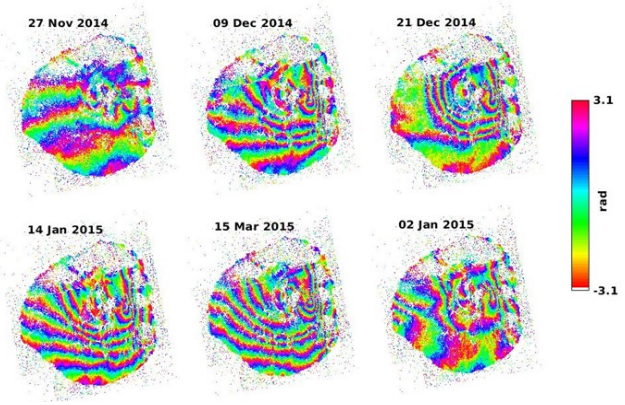

Figure. 3. Wrapped Interferograms

PSInSAR technique is applied to 7 Sentinel-1A SAR images acquired in ascending pass from November 2014 to March 2015. From these datasets, 6 interferograms are computed using the method described in the previous section. The Fogo volcano area is covered in the IW 2, so the PSInSAR method is applied this sub-swath only.

The Figure. 3 shows the wrapped interferograms of each slave image with respect to the master image of 3rd November 2014. The wrapped interferograms contain phase contributions due to the spatially correlated look angle error, atmosphere and orbital errors. From the interferogram of 27th November, it can be seen that except for the Fogo volcano area all other areas are having broad interferogram fringes indicating no surface deformation. The Fogo volcano area is having discontinuous elliptical interferogram fringes indicating surface deformations. The interferogram of 9th December shows the formation of circular discontinuous fringes indicating spreading deformation to more areas. The interferograms of 21st December and 2nd January shows clear circular discontinuous interferogram fringes showing the spread of deformation. Interferometric fringes in the interferograms of 14th January and 15th March are almost same indicating reduced volcano activities.

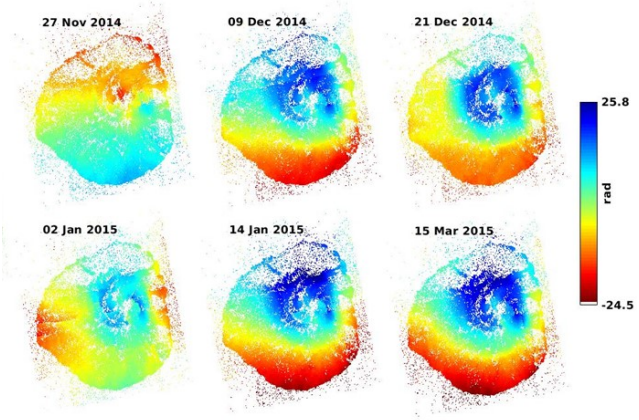

Figure. 4. Unwrapped Interferograms

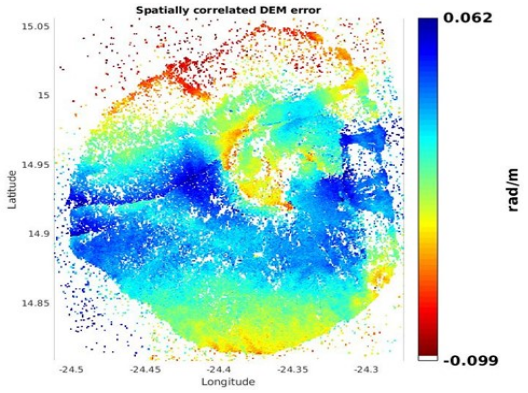

Figure.5. Spatially Correlated Topographic phase

The unwrapped interferograms (Figure. 4) justify the information extracted from the wrapped interferograms. The change in the phase of the interferograms can be observed from 27th November to 14th January indicating surface deformation due to volcanic activities. In the interferogram of 27th November, the areas near the Fogo volcano are having yellow to a cyan colour indicating only very small phase change with respect to 3rd November except the volcano crater which can be seen in red colour at the middle of the image indicating high negative phase difference. The interferograms of 9th December and 21st December shows high phase difference at the volcano area indicated by blue colour. High volcanic activity and the resulting lava flow is the reason for the high phase difference in these areas. From the interferogram of 2nd January, it can be seen that the phase difference is considerably reduced indicating reduced volcanic activity. But the interferogram of 14th January again shows high phase difference at the volcano areas indicating regained volcano activities. The unwrapped interferograms of 14th January and 15th March are almost same indicating no surface deformation during this period and the halt of volcanic activities.

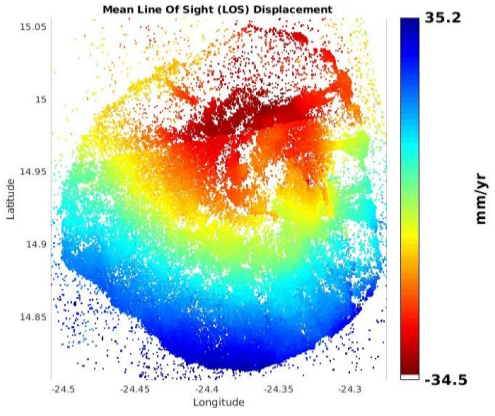

Figure. 6. Mean LOS Displacement

Figure. 5. Shows the spatially correlated topographic phase component. It is estimated by low pass and high pass filtering of master and slave images respectively. This estimated phase is then subtracted from the unwrapped phase of all interferograms to obtain the phase only due to surface deformation.

The Mean Line of Sight Displacement (Figure. 6.) of the Fogo volcano area from 3rd November to 15th March shows that there occurred a displacement of -3.45 cm at the Fogo Volcano crater due to the subsidence caused by volcanic activities indicated by the red colour. The yellow and cyan coloured regions are having a displacement of around 1 to 2 cm. Green colour indicates regions having zero displacements. Blue coloured regions are having a LOS displacement of approximately +3.5 cm. The volcano activity and Lava flow occurred towards the northwestern regions of the volcano crater indicating high LOS displacement towards these regions.

Figure. 7. Shows the standard deviation image of the mean LOS Displacement. It can be seen that the areas in red colour are less affected by the volcano activities indicated by the low standard deviation in the range of 2.2 cm/year. The low standard deviation is due to the low or near similar displacement rate in different interferograms. The other areas are having high standard deviation extending up to 3.0 cm/year due to the variation in displacement rate in different interferograms. The high standard deviation towards the North West side of the volcano crater shown in cyan and blue colour indicates the varying displacement rates due to the lava flow where the Portela and Bangaeria villages are situated.

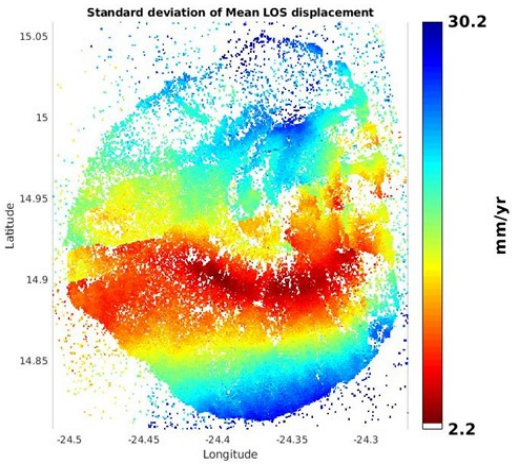

Figure. 7. Standard Deviation of Mean LOS Displacement

4. Conclusions

The surface deformation of Fogo volcano areas due to the volcanic eruption is estimated using the PSInSAR technique in this research. PSInSAR technique used a large number of datasets to precisely estimate and remove the phase errors due to atmosphere and topography. The selection of PS pixels using both amplitude stability and phase stability ensured a high density of PS pixels the natural terrain free from any stable manmade structures. The absence of thick vegetation helped in preventing decorrelation to the interferograms. There occurred a displacement in the range of -34 mm to +35 mm to the Fogo volcano areas due to the volcanic episode. The high standard deviation of LOS displacement at the volcano areas indicates deformation to the terrain.

Conflicts of Interest: The authors declare no conflict of interest.

References

1. A. Ferretti, C. Prati, and F. Rocca, "Permanent Scatters in SAR Interferometry," *IEEE Trans. Geosci. Remote Sens.*, vol. 39, no. 1, pp. 8–20, 2001.
2. M. Even and K. Schulz, "InSAR deformation analysis with distributed scatterers: A review complemented by new advances," *Remote Sens.*, vol. 10, no. 5, 2018.
3. A. Hooper, H. Zebker, P. Segall, and B. Kampes, "A new method for measuring deformation on volcanoes and other natural terrains using InSAR persistent scatterers," *Geophys. Res. Lett.*, vol. 31, no. 23, pp. 1–5, 2004.
4. A. Hooper, P. Segall, and H. Zebker, "Persistent scatterer interferometric synthetic aperture radar for crustal deformation analysis, with application to Volcán Alcedo, Galápagos," *J. Geophys. Res. Solid Earth*, vol. 112, no. 7, 2007.
5. T. S. Peltier, A., M. Bianchi, E. Kaminski, J.-C. Komorowski, A. Rucci, "PSInSAR as a new tool to monitor pre-eruptive volcano ground deformation: Validation using GPS measurements on Piton de la Fournaise," *Geophys. Res. Lett.*, vol. 37, no. 12, 2010.
6. N. Richter *et al.*, "Lava flow hazard at Fogo Volcano , Cabo Verde , before and after the 2014 – 2015 eruption," no. January 2002, pp. 1925–1951, 2016.
7. S. J. Day, S. I. N. Heleno da Silva, and J. F. B. D. Fonseca, "A past giant lateral collapse and present-day flank instability of Fogo, Cape Verde Islands," *J. Volcanol. Geotherm. Res.*, vol. 94, no. 1–4, pp. 191–218, Dec. 1999.
8. N. Yague-martinez *et al.*, "Interferometric Processing of Sentinel-1 TOPS Data," vol. 54, no. 4, pp. 2220–2234, 2016.
9. P. J. González *et al.*, "The 2014–2015 eruption of Fogo volcano: Geodetic modeling of Sentinel-1 TOPS interferometry," pp. 9239–9246, 2015.
10. P. Gonnuru and S. Kumar, "PsInSAR based land subsidence estimation of Burgan oil field using TerraSAR-X data," *Remote Sens. Appl. Soc. Environ.*, vol. 9, no. September 2017, pp. 17–25, 2018.
11. A. Sharifuddin, A. Matori, A. Aobpaet, and A. Hassan, "Monitoring of Offshore Platform Deformation with Stanford method of persistent scatterers (StaMPS)," in *International Conference on Space Science and Communication*, 2015.